Combinatorial Optimization of La, Ce-co-Doped Pyrosilicate Phosphors as Potential Scintillator Materials

Qinhua Wei,[†,‡] Jieqiong Wan,[†,‡] Guanghui Liu,[†] Zhenzhen Zhou,[†] Hua Yang,[†,‡] Jiacheng Wang,[†] and Qian Liu*,[†]

[†]State Key Laboratory of High Performance Ceramics and Superfine Microstructure, Shanghai Institute of Ceramics, Chinese Academy of Sciences, Shanghai 200050, China

[‡]Graduate University of the Chinese Academy of Sciences, Beijing 100049, China

ABSTRACT: A combinatorial method was employed to rapidly screen the effects of La, Ce-co-doping on the luminescent properties of $Gd_2Si_2O_7$ pyrosilicate using an 8×8 library. The candidate formulations $(Gd_{1-x-y}La_x)_2Si_2O_7{:}Ce_{2y}$ were evaluated by luminescence pictures under ultraviolet excitation. The optimal composition was found to be $(Gd_{0.89}La_{0.1})_2Si_2O_7{:}Ce_{0.02}$ after scaled-up preparation and detailed characterization of powder samples, which shows an excellent light output under both ultraviolet and X-ray excitation (about 5.43 times of commercial YAG:Ce powders). The XRD results indicate that the phase structure sequence is tetragonal−orthorhombic−triclinic for different calcination temperatures and doping ions. The $(Gd_{0.89}La_{0.1})_2Si_2O_7{:}Ce_{0.02}$ powder sample also demonstrated excellent temperature stability of luminescence up to 200 °C and a short decay time of several tens of nanoseconds, suggesting that this may represent a new kind of scintillation material, such as single crystals, ceramics, glass, or phosphors.

KEYWORDS: ceramic phosphors, combinatorial screening, inkjet printing, luminescence, thermo-stability
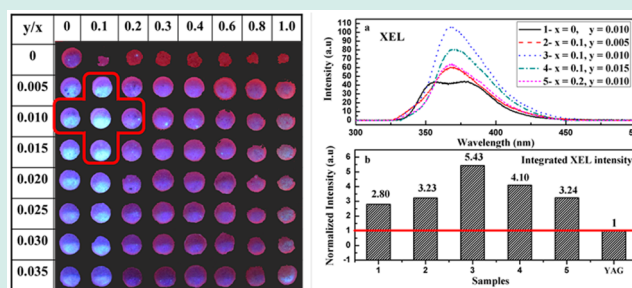
■ INTRODUCTION

Silicate light absorbing and emitting materials have a number of advantages, including high density and Z_{eff} (effective atomic number) values, good chemical stability, high light yield, and fast luminescence decay. The industrial production of detectors based on oxyorthosilicate single crystals, including $Gd_2SiO_5{:}Ce$ (GSO:Ce),[1] $Lu_2SiO_5{:}Ce$ (LSO:Ce),[2] and $(Lu,Y)_2SiO_5{:}Ce$ (LYSO:Ce),[3] has been widely applied in many fields. However, LSO:Ce and LYSO:Ce exhibit the intrinsic background signal of ^{176}Lu, while GSO:Ce has a low value of background signal. Thus, GSO:Ce can be used in low signal count rate environments such as gamma-ray astronomy or in Compton cameras.[4,5] Recently, cerium doped gadolinium pyrosilicate, $Gd_2Si_2O_7{:}Ce$ (named as GPS:Ce) has attracted great attention,[6−8] because of its much lower afterglow level, much higher light output, and shorter decay time than those GSO:Ce. Furthermore, the Gd thermal neutron capture cross-section and the light yield of GPS:Ce under thermal neutrons were shown to be twice that of GSO:Ce,[9,10] making GPS:Ce a greatly attractive. Additionally, GPS:Ce crystals show an absence of luminescence quenching over a wide temperature range: triclinic GPS:Ce retains 80% of its room-temperature luminescence intensity up to 470 K and is characterized by an increase of luminescence yield by 10−20% at temperatures from room temperature up to 365 K.[11,12] This is an important advantage of GPS:Ce for applications under severe temperature conditions such as well logging, nuclear stations, etc.

Unfortunately, it has been found that the composition $Gd_2Si_2O_7$ (or $Gd_2O_3{-}2SiO_2$) is not congruent in the $Gd_2O_3{-}SiO_2$ binary system and high quality crystals are difficult to be obtained with heavy doping of Ce^{3+} ions.[13,14] Such high Ce concentrations lead to severe reabsorption of luminescence and possible deterioration of scintillation characteristics because of concentration quenching effects. A new approach for solving these problems is to substitute cerium by optically inactive lanthanum,[15,16] since the La^{3+} ion has a similar ionic radius to Ce^{3+} and the substitution of La for Ce can stabilize the pyrosilicate phase. In this way, concentration quenching can be efficiently avoided by moderate reduction of Ce doping. Recently, La-co-doped single crystal scintillators, $(Gd_{1-x-y}La_x)_2Si_2O_7{:}Ce_{2y}$ (La-GPS:Ce), were successfully grown by floating zone (FZ), top seeded solution (TSSG), and Czochralski methods under argon atmosphere,[11,15−17] showing a high energy resolution of approximately 5% and high light yield under either γ-rays or thermal neutrons. However, previous work has only focused on a limited number of concentrations, making the effects of La^{3+} codoping on the luminescence properties of GPS:Ce and the optimized doping concentration unclear.

The initial intent of our work was focused on the combinatorial screening of compositions in La-GPS:Ce system to show a relationship between composition and emission intensity. This may provide useful recipe information for scintillator materials, including phosphors, ceramics, and single crystals. Three forms of La-GPS:Ce materials have attracted recent attention, and such ceramics usually possess a higher doping-tolerance comparing to single crystals. In addition, the luminescence properties of single crystals are quite different from ceramics and powders in process routing and dopant concentrations. Thus, far, studies on ceramics, powders, or ceramic composites of La-GPS:Ce are rare. Here we report the combinatorial optimization of both La-for-Gd replacement and Ce doping in the general composition $(Gd_{1-x-y}La_x)_2Si_2O_7:Ce_{2y}$.

Fast combinatorial chemistry methods provide useful tools for the discovery and development of new materials, an important objective highlighted by the Materials Genome Initiative.[18] Our findings described here of optimized La-GPS:Ce compositions are almost identical to those reported previously in references 11, 15, 16, and 17. This correspondence provides strong support both for the validity of our screening method and for the previous findings, which did not survey as large a variation in potential compositions. The appropriateness of combinatorial synthesis and screening of films or powders has been questioned for bulk materials (glass, ceramics, and crystals) for many years. While this report cannot address all such concerns, we do show that a combinatorial approach can be useful tool to screen and obtain "optimized" phosphor compositions either in the context of new materials or to enhance confidence in previous results.

In our experiment, an 8×8 library of candidates was synthesized using an automatic liquid injector to dispense the desired components in a block array of cells. The library samples were then calcined to form La-GPS:Ce ceramic powders and evaluated by screening of luminescence intensity under UV illumination. The best compositions, identified by the observed brightness of emission, were synthesized on a larger scale by sol−gel processing under the same experiment conditions as those used for the library preparation. The resulting powder samples were analyzed in detail to characterize their photoluminescence characteristics, X-ray luminescence, decay time, and temperature quenching effect.

◼ EXPERIMENTAL PROCEDURES

A series of La-GPS:Ce material libraries were prepared using a drop-on-demand inkjet delivery system (model CIJ, fabricated by the University of Science and Technology of China, Hefei, China),[19,20] and just one of them was chosen showing in this paper, as well as for the larger scale synthesis. To keep a small composition step controllable, the raw materials used in the synthesis are as follows: Gd-, La-, and Ce-containing solutions were prepared by dissolving Gd_2O_3 (99.99%), La_2O_3 (99.99%) in nitric acid (AR) and $Ce(NO_3)_3$ (AR) in deionized water, respectively. The Si-solution was prepared by dissolving TEOS (AR) in ethanol. The details about the solutions used in the precursor delivery are summarized in Table 1. Before ejection, the solutions were infused with argon gas for 3 h to expel any air dissolved in the suspension which has a tendency to agglomerate and block the nozzle. Then the accurate amount of each solution was collected in the ceramic microreactors of 8×8 cells with the assistance of a computer programmed injection system according to the designed composition map. The diameter of cell is 8 mm and the depth of cell is about 8 mm.

Table 1. Details about the Solutions Used in Precursor Delivery

raw material	purity	solution	concentration (M)
TEOS	AR	ethanol	1
Gd_2O_3	99.99%	20% HNO3	1
La_2O_3	99.99%	20% HNO3	1
$Ce(NO_3)_3$	AR	Deionized water	0.05

The solutions in the microreactors were agitated in an ultrasonic bath for 2 h and then dried at 80 °C for 24 h. The mixed solution turned into a gel state at this stage and then was calcined at 600 °C for 2 h in a weak reducing atmosphere produced by an incomplete oxidation of activated carbon. Finally, these 64 powder samples filled in cells were subsequently heat treated at higher 1400 °C in the same atmosphere. The utilization of weak reducing atmosphere produced by an incomplete oxidation of activated carbon is to avoid the oxidation of Ce^{3+} to Ce^{4+}, and that treatment has no effect on the final product composition. The detail can be found in previous report.[21] then, the prepared library was excited with Hg lamp possessing a 365 nm broadband filter, and the photoluminescence intensity of the small samples in the library was recorded using a digital camera.

According to the recorded image of luminescence, the preferred compositions showing higher intensity or brightness were selected as "clue" and independently synthesized on a larger scale by sol−gel method under the same conditions as the library's preparation for further investigation. The crystal structure and phase purity of the powder samples were analyzed by X-ray diffraction (XRD) with Cu Kα radiation (λ = 0.1541 nm). The photoluminescence (PL) spectra and photoluminescence excitation (PLE) spectra of the powders under UV light were recorded on a Hitachi F-4600 spectrometer. The temperature dependence of PL intensity was also measured in a range from room temperature (RT) to 200 °C. All of the samples were the same mass and pressed into disks with the same dimensions of approximately Ø20 mm × 1 mm for measuring the photoluminescence spectrum. The slits for both excitation and emission measurement were all set as 2.5 nm and the scan speed was fixed at 240 nm/min. The radioluminescence spectra were conducted on an X-ray Excited Luminescence Spectrometer, in which X-ray tube was operated at the condition of V = 70 kV and I = 2 mA. The decay time was studied with the FLS920 spectrofluorometer for nanosecond.

◼ RESULTS AND DISCUSSION

The designed composition map and recorded luminescent images of the $(Gd_{1-x-iy}La_x)_2Si_2O_7:Ce_{2y}$ library under UV excitation of 365 nm are both shown in Figure 1. The 8×8 array consists of 64 compositions with La^{3+} and Ce^{3+} contents varied from x = 0 to 1.0 and y = 0 to 0.035 (Figure 1). The powder samples on the library were all calcined under the optimal condition of 1400 °C for 4 h. The lamp light was illuminated evenly over the library, so that a relative comparison could be made among the samples in the library. From Figure 1, it can be seen that the illumination of samples is not well homogeneous and there are some dark points. Usually, the luminance is related with the degree of dispersion of samples, it is suspected that the inhomogeneous illumination of some points results from the particle aggregation. But we can found that the dark or bright points are few and have no effect
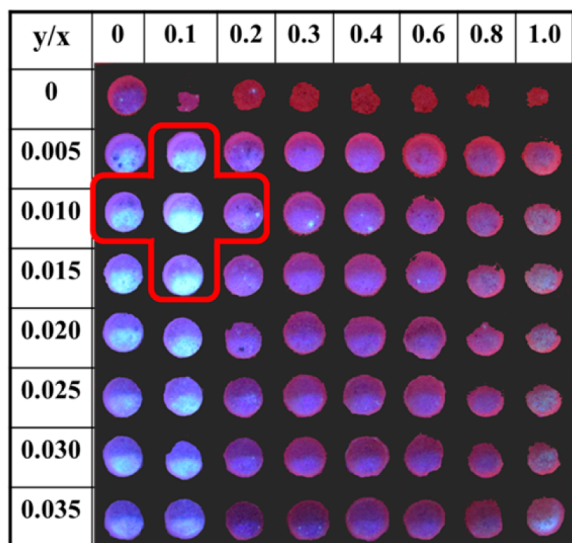
Figure 1. Designed composition map and recorded photoluminescence photography of the $(Gd_{1-x-y}La_x)_2Si_2O_7:Ce_{2y}$ library excited under 365 nm UV light, with $x = 0-1.0$ and $y = 0-0.035$.

on the result. Besides, the dark color in some cells is just from the shadow when taking the photo. Meanwhile, it is obvious that the brighter luminescent composition points appear on the left area of the composition map and the intensities rapidly decrease when the replacement content of La for Gd exceeds 0.1 ($x = 0.1$). Taking a transverse contrast, the concentration quenching is also observed with the Ce content (y) exceeding ~0.010, where the higher photoluminescence compositions are identified at $x = 0.1$ and $y = 0.005-0.015$, those are the points of ($x = 0.1$, $y = 0.005$), ($x = 0.1$, $y = 0.010$), ($x = 0.1$, $y = 0.015$) points in the 8×8 array. To confirm the effect of La^{3+} ions replacement on the compound, the compositions at x = 0, y = 0.010 and x = 0.2, y = 0.010 were also chosen as the interesting or preferred clue compositions. The five clue compositions are strikingly shown in the red frame circled region marked in Figure 1 and the clue compositions are used for further evaluation to the synthesized powders on a larger scale product. The scale-up powder samples were prepared through a sol–gel reaction under the same experimental conditions as the library's preparation.

To study the phase formation process of the prepared powder samples, the XRD patterns of both GPS:Ce ($Gd_{2(1-y)}Si_2O_7:Ce_{2y}$) and La-GPS:Ce (($Gd_{1-x-y}La_x)_2Si_2O_7:Ce_{2y}$) samples calcined at 600, 1100, 1200, 1300 and 1400 °C in a weak reduce ambience were tested and are showing in Figure 2, along with the corresponding amorphous phase, standard XRD patterns of Gd_2O_3 (PDF no. 43-1014), $Gd_{9.33}(SiO_4)_6O_2$ (PDF no. 38-0283), and $Gd_2Si_2O_7$ (ICSD-98723 and PDF no. 24-0065) as well. As shown in Figure 2a for La-free samples' XRD analysis, it can be clearly found that there are four different crystallized phases prepared at different calcination temperatures and the product calcined at 1100, 1200, 1300, and 1400 °C is corresponding to Gd_2O_3, $Gd_{9.33}(SiO_4)_6O_2$, and $Gd_2Si_2O_7$ tetragonal phase, and $Gd_2Si_2O_7$ orthorhombic phase, respectively. XRD results show that the sample calcined at higher 1300 and 1400 °C has been well crystallized and owns two different structures of $Gd_2Si_2O_7$ (ICSD-98723 and PDF no. 24−0065) phase. Obviously, the tetragonal phase is a low-temperature metastable phase. Herein, the samples, calcined at 1400 °C, are being studied.

The formation sequence on calcination as shown in Figure 2a based on XRD data indicates that the amorphous phase can be obtained at 600 °C for 2 h and the gadolinium oxide can be observed at 1100 °C, so the reaction temperature of Gd_2O_3 and SiO_2 is above 1100 °C and the crystalline temperature of gadolinium oxide is lower than the reaction temperature of GPS. In our experiment, the orthorhombic can be observed for GPS:Ce at 1400 °C, which is agree with the standard XRD patterns, and that is stable when it cooled from the 1400 °C to RT. But, according to previous works that the orthorhombic form of pure GPS is a high temperature form usually observed above 1430 °C, we suspect that the phase form temperature is related with the synthesis method, heating equipment and raw material, therefore, the orthorhombic form of GPS:Ce obtained at 1400 °C is reasonable.

In this Research Article, the GPS:Ce powders obtained at 1400 °C are identified to be an orthorhombic phase and its space group is Pna21. Based on the results of XRD patterns, it is a reasonable speculation that the $Gd_2Si_2O_7$ phase formation procedure usually follows a three-step, that is the low temperature pyrogenation phase (Gd_2O_3) formation, hexagonal phase ($Gd_{9.33}(SiO_4)_6O_2$) formation, and orthorhombic phase
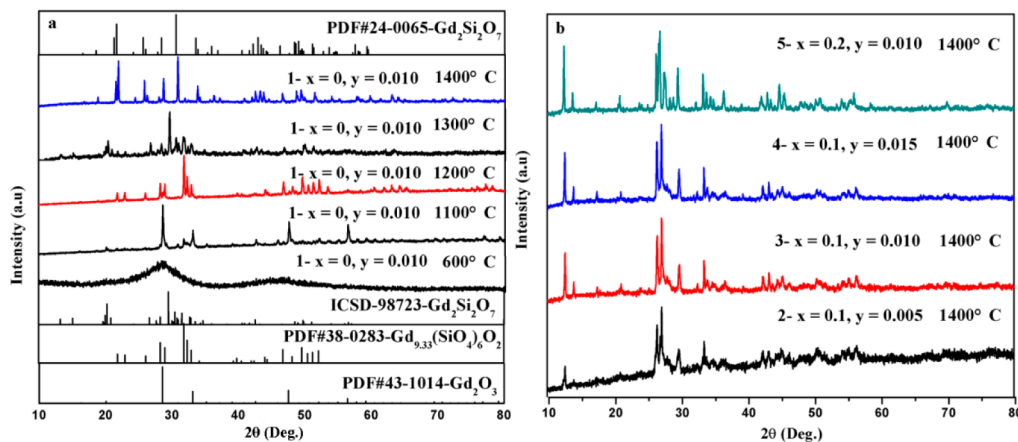

Figure 2. (a) XRD patterns of $Gd_2Si_2O_7:Ce_{2y}$ ($y = 0.010$) samples calcined at 600, 1100, 1200, 1300, and 1400 °C in a weak reduce ambience, along with the standard XRD spectra of Gd_2O_3, $Gd_{9.33}(SiO_4)_6O_2$, and $Gd_2Si_2O_7$ phase. (b) XRD patterns of four $(Gd_{1-x-y}La_x)_2Si_2O_7:Ce_{2y}$ ($x = 0.1$, $y = 0.005$, 0.010, and 0.015; $x = 0.2$, $y = 0.010$) samples calcined at 1400 °C in a weak reduce ambience.

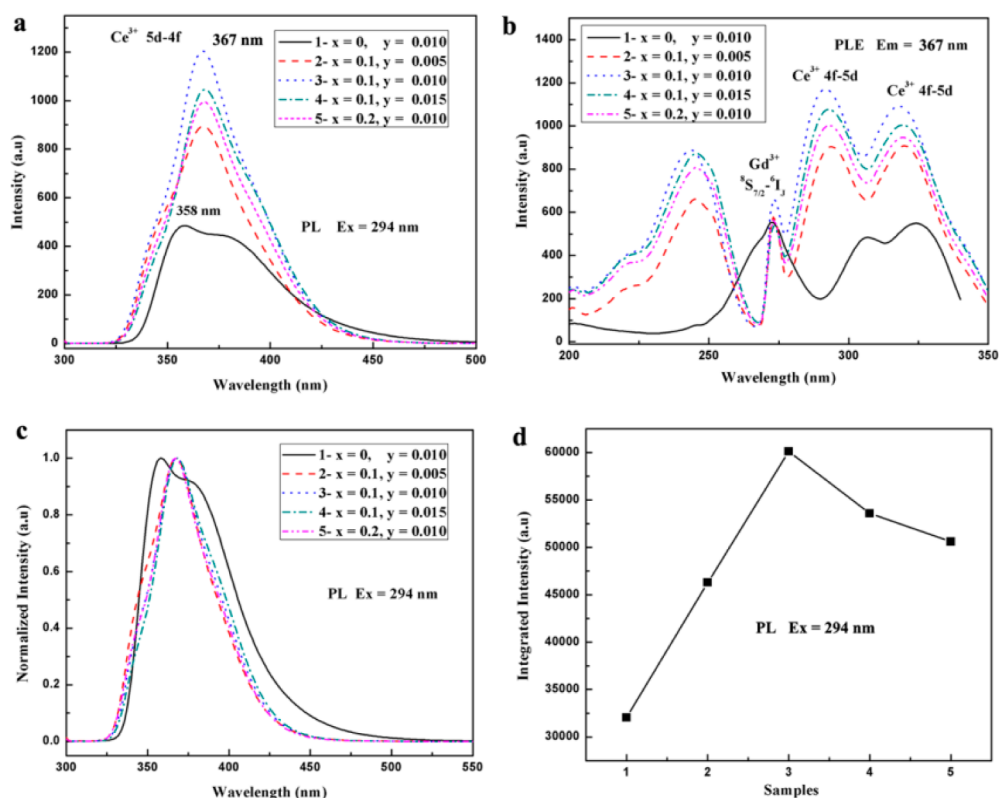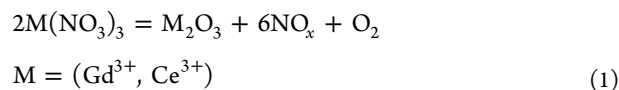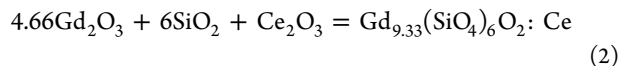**Figure 3.** (a) Emission (λ_{ex}= 294 nm) and (b) excitation (λ_{em}= 367 nm) spectra measured at room temperature, (c) normalized PL spectra, and (d) dependence of integrated emission intensity of the five $(Gd_{1-x-y}La_x)_2Si_2O_7$:$Ce_{2y}$ phosphor samples, in which $x = 0$, $y = 0.010$ (sample 1); $x = 0.1$, $y = 0.050$, 0.010, and 0.015 (samples 2, 3, and 4); $x = 0.2$, $y = 0.010$ (sample 5).

$(Gd_2Si_2O_7)$ formation. The three-step reaction can be expressed in following equations:

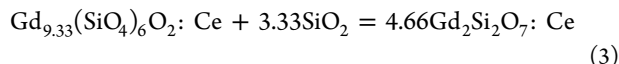pyrogenation phase formation (600−1100 °C)

$$2M(NO_3)_3 = M_2O_3 + 6NO_x + O_2$$

$$M = (Gd^{3+}, Ce^{3+}) \tag{1}$$

hexagonal phase formation (1200 °C)

$$4.66Gd_2O_3 + 6SiO_2 + Ce_2O_3 = Gd_{9.33}(SiO_4)_6O_2: Ce \tag{2}$$

orthorhombic phase formation (1400 °C)

$$Gd_{9.33}(SiO_4)_6O_2: Ce + 3.33SiO_2 = 4.66Gd_2Si_2O_7: Ce \tag{3}$$

The XRD patterns of the four clue compositions $(Gd_{1-x-y}La_x)_2Si_2O_7$:$Ce_{2y}$ ($x = 0.1$, $y = 0.050$, 0.010, and 0.015; $x = 0.2$, $y = 0.010$), calcined at 1400 °C in a weak reduce ambience, are shown in Figure 2b. The figure shows a different result from Figure 2a. The XRD results of La-GPS:Ce obtained at 1400 °C for 4h are consistent with the refs 11, 15, and 16, and that phase had a triclinic structure with $P\bar{1}$ space group and the La-GPS structure was identical to that of triclinic GPS. So, we can found that the structure sequence is tetragonal−orthorhombic-triclinic, the tetragonal is a metastable phase. Besides, the crystallinity of powders becomes better as the concentration of La^{3+} raises. On the basis of the results, we can give a conclusion that the triclinic phase is obtained for the La^{3+} ion codoping samples in our experiments. The detail of phase transition and reaction mechanism is quite complicated and will be discussed in a separated paper later.

Emission (λ_{ex} = 294 nm) and excitation (λ_{em} = 367 nm) spectra of scale-up produced $(Gd_{1-x-y}La_x)_2Si_2O_7$:$Ce_{2y}$ phosphors are shown in Figure 3a and 3b (measured at room temperature), while the dependence of integrated emission intensity on La^{3+} and Ce^{3+} concentrations and normalized PL spectra of $(Gd_{1-x-y}La_x)_2Si_2O_7$:$Ce_{2y}$ samples are shown in Figure 3c and 3d. It has to be emphasized that the compositions design of the selected five scale-up samples is corresponding to the content variety of doping ions ($x = 0$, $y = 0.010$; $x = 0.1$, $y = 0.005$, 0.010, and 0.015; $x = 0.2$, $y = 0.010$), in which three composition points ($x = 0.1$, $y = 0.005$, $y = 0.010$ and 0.015) are directly related to the brighter points on the screening map under UV excitation (Figure1). Obviously, a broad emission band from Ce^{3+} emission can be observed in Figure 3a and 3c, and both the shape and position of emission spectra are not changed with the variation of La concentrations for the La-co-doping sample (La-GPS:$Ce_{0.02}$), except the emission intensity fluctuation. However, the emission peaks are at 358 and 385 nm for La-free sample GPS:$Ce_{0.02}$, while a single peak at 367 nm is for the La-co-doping sample. Moreover, the excitation spectra also show a sharp variation for the La-co-doped compositions contrary to La-free composition, as illustrated in Figure 3b. The excitation spectra have a shift toward shorter wavelength and two new excitation peaks located at 200−250 nm can be observed for the La-co-doping samples. The new peaks of excitation can be assigned to relate with crystal structure and La^{3+} ions. The other three peaks at around at 272, 294, and 320 nm are ascribed to the $^8S_{7/2}-^6I_J$ electron transition of Gd^{3+} and 4f-5d electron transition of Ce^{3+}, respectively. The evident blue shift of excitation peaks (at 294 and 320 nm) may result from a change

in energy levels of light active Ce^{3+} ion caused by the variation of crystal field with increasing of codoped La^{3+} content, which is expected to distort the lattice cell due to the occupation of La^{3+} in Gd^{3+} sites, because the crystal structure has been changed from orthorhombic structure of GPS phase to triclinic one of La-GPS:Ce phase, with the codoping of La ions in GPS:Ce compositions as shown in Figure 2a and b. To compare the emission intensity change with the varied content of Ce and La ions in GPS, the PL spectra were integrated. The integrated results are depicted in Figure 3d for the five scale-up prepared powder samples. The integrated PL intensity of $(Gd_{1-x-y}La_x)_2Si_2O_7:Ce_{2y}$ samples is increased sharply at first from the sample 1 to sample 3, reaching a maximum value at composition of $x = 0.1$, $y = 0.010$, and then decreased for the sample 4 and sample 5, with compositions of $x = 0.1$, $y = 0.015$ and $x = 0.2$, $y = 0.010$, respectively, which exactly coincides with the combinatorial screening results (indicated in Figure 1). Thus, these data on PL intensities of scaled-up samples demonstrate that the $(Gd_{0.89}La_{0.1})_2Si_2O_7:Ce_{0.02}$ ($x = 0.1$, $y = 0.010$) is the optimum composition with the highest emission among those tested.

The emission spectra recorded at room temperature under X-ray excitation for the five $(Gd_{1-x-y}La_x)_2Si_2O_7:Ce_{2y}$ powder samples are presented in Figure 4a. In our experiments the
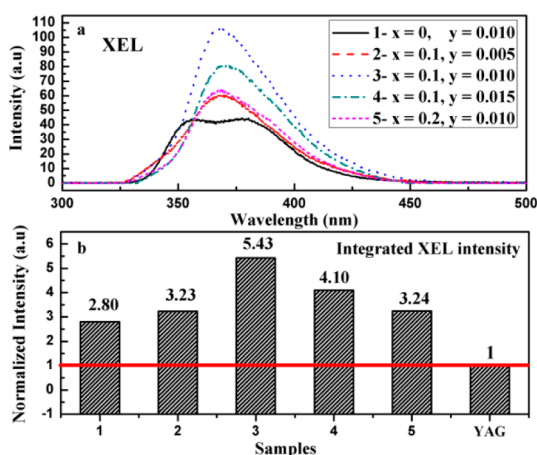

Figure 4. X-ray excited luminescence spectra of $(Gd_{1-x-y}La_x)_2Si_2O_7:Ce_{2y}$ ($x = 0.1$, $y = 0.005$, 0.010, 0.015; $x = 0$, 0.2, $y = 0.010$) powders, measured at room temperature (a), and relative integrated intensity of $(Gd_{1-x-y}La_x)_2Si_2O_7:Ce_{2y}$ comparing to YAG:Ce reference sample (b).

commercial YAG:Ce powder emission spectrum has also been recorded to evaluate the luminescence intensity of $(Gd_{1-x-y}La_x)_2Si_2O_7:Ce_{2y}$ powder. The La-co-doping samples present a dominated emission band peaking at 367 nm, while the emission of GPS:Ce sample shows a hump characteristic peaking at 358 and 385 nm, respectively, which is well in agreement with that of PL spectrum under UV radiation. The X-ray excited light output of the five $(Gd_{1-x-y}La_x)_2Si_2O_7:Ce_{2y}$ samples were determined by the ratio of integrated intensity $I_{(La-GPS:Ce)}$ to that of YAG:Ce reference sample. On th basis of the integration value of the Ce^{3+} emission intensity in radioluminescence spectra (XEL), the relative light output has been calculated and compared with that of YAG:Ce. According to the results shown in Figure 4b, the light output of $(Gd_{1-x-y}La_x)_2Si_2O_7:Ce_{2y}$ samples is also increased sharply at first from the sample 1 to sample 3, reaching a maximum value

at composition of $x = 0.1$, iy = 0.010, and then decreased for the sample 4 and sample 5, with compositions of $x = 0.1$, $y = 0.015$ and $x = 0.2$, $y = 0.010$, respectively. The light output of the sample 3 with an optimum composition ($x = 0.1$, $y = 0.010$) is about 5.43 times of commercial YAG:Ce powders' output value. Besides that the sample 1 of undoped La ions presents a lower light output under X-ray excitation. On the basis of the above analysis, we tentatively speculate that the La ions doping contributes positive effects on the light output enhancement of GPS:Ce phosphors. In comparison with published literatures, the previous work just focused on one concentration or several concentrations of single crystal and it was hard to give an "optimized" composition, while our work mainly focused on the combinatorial screening. Actually, our experiments results are obtained almost at the same time with the reports published in refs 16 and 17. Compared to the experiment results, we know that our "optimized" final phosphor composition is almost identical to the compositions formerly tested in the previous literatures,[11,15−17] Which proofs that our screening result is reasonable, and the combinatorial chemistry method is effective, significance, and important for the design of new "luminescent" single crystals or ceramics, by establishing a primary relationship between composition−structure−property (emission). Besides, the results of previous literature are also reliable. Herein, we also emphasize that the combinatorial screening is not only a study method to discover new materials with optimized properties, but also a good way to verify or check the previous work in case of any omission of probable compositions, especially, for the ceramic or phosphors.

Both PL and PLE spectra of the optimal composition $(Gd_{0.89}La_{0.1})_2Si_2O_7:Ce_{0.02}$ phosphors (sample 3) are shown in Figure 5a, and the high energy X-ray excited luminescence
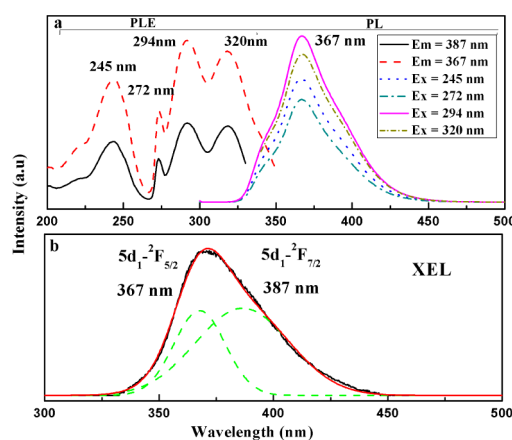

Figure 5. PLE and PL spectra of the optimal composition $(Gd_{0.89}La_{0.1})_2Si_2O_7:Ce_{0.02}$ sample (a), and XEL spectrum (b), recorded at room temperature.

(XEL) spectrum is separately presented in Figure 5b, recorded at room temperature. There are four dominated PLE peaks at 245, 272, 294, and 320 nm monitored at either 367 or 387 nm. The four dominated PLE peaks are ascribed to $^8S_{7/2}-^6I_J$ electron transition of Gd^{3+}, and 4f−5d electron transition of Ce^{3+}, respectively, as discussed above for explaining Figure 3a. An asymmetry peak in PL and XEL spectrum, located at 367 nm, can be detected under different excitation wavelengths. Through Gaussian fitting, the asymmetry peak can be decomposed into two peaks centering nearly at 367 and 387 nm, respectively, as shown in Figure 5b, corresponding to the

Ce^{3+} electron transition from lowest 5d level to $^2F_{5/2}$ and $^2F_{7/2}$ of 4f sublevels. The shape and emission peak of XEL are well in agreement with that of PL spectrum under UV radiation.

The optimal $(Gd_{0.89}La_{0.1})_2Si_2O_7:Ce_{0.02}$ sample was also chosen to measure its fluorescence decay time at room temperature (RT). The RT fluorescence decay curve under the optimal excitation and emission wavelength (λ_{em} = 367 nm, λ_{ex} = 294 nm) is shown in Figure 6. It is well established that
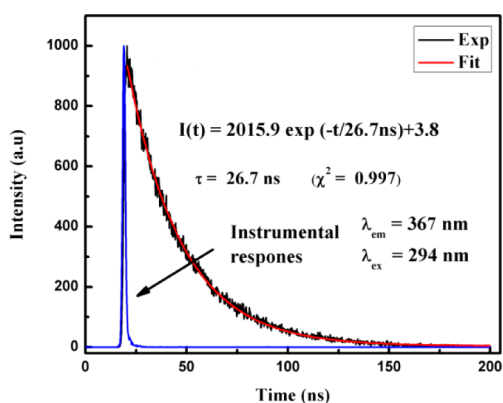

Figure 6. Decay curve of the optimal composition $(Gd_{0.89}La_{0.1})_2Si_2O_7:Ce_{0.02}$ powders measured at room temperature (monitoring excitation and emission wavelength are fixed at 294 and 367 nm, respectively).

the decay behavior of the $(Gd_{0.89}La_{0.1})_2Si_2O_7:Ce_{0.02}$ sample can be expressed by

$$I(t) = I_0 \times \exp(-t/\tau) \qquad (4)$$

where I_0 denotes the intensity of emission at $t = 0$ and τ is the decay constant. Basically, τ depends on the mechanism of electronic transition at the emission center. On the basis of eq 4 and decay curve, the fitting decay time of $(Gd_{0.89}La_{0.1})_2Si_2O_7:Ce_{0.02}$ sample is found to be about 26.7 ns. Comparing to the decay time (30−42 ns) of La-GPS:Ce single crystal,[15] the decay time of the powder sample is reasonable and approximate.

Previously, it was shown that the lutetium and gadolinium pyrosilicates demonstrate a good thermal stability of light output in a wide temperature range.[11,22,23] In the present work, the varied temperatures PL spectra (λ_{ex} = 294 nm) of the $(Gd_{0.89}La_{0.1})_2Si_2O_7:Ce_{0.02}$ powders were also measured from RT to 200 °C, as shown in Figure 7, the inset is the temperature dependence of integrated emission intensity of samples. Viewed from Figure 7, we can found that the decrease in emission intensity and broadening of fwhm are apparent upon heating and these changes can be explained by the thermal quenching at configurational coordinate diagram. With increasing of temperature, it must cause an evident increase in the nonradiative transition probability by thermal activation and release of the luminescent center through the crossing point between the excited state and the ground state. It is the increase of nonradiative transition and release of luminescent centers that quenches the luminescence. In the quenching process, the electron phonon interaction is enhanced at high temperatures as a result of the increased population density of phonon, which broadens fwhm of PL spectra. The integral emission intensity, proportional to the quantum efficiency, decreases slightly less than the peak intensity dropping. Usually, the thermal quenching temperature T_{50} is defined as the temperature at
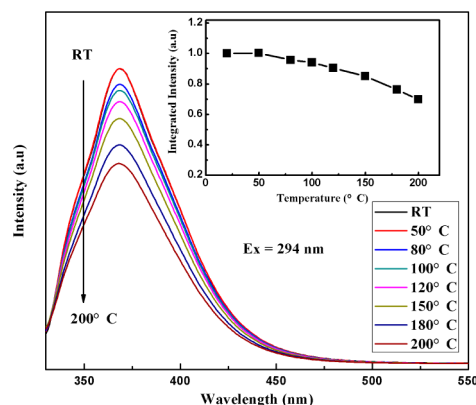

Figure 7. Emission spectra of the optimal composition $(Gd_{0.89}La_{0.1})_2Si_2O_7:Ce_{0.02}$ powders heated from RT to 200 °C, the inset is the temperature dependence of integrated emission intensity.

which the emission intensity is 50% of its RT value.[24] It has been noticed that a good result was obtained for the optimal $(Gd_{0.89}La_{0.1})_2Si_2O_7:Ce_{0.02}$ sample keeping its 70% RT emission intensity when temperature up to 200 °C. In addition, the emission peak position shows no shift as the temperature raise. This is an important advantage for the future applications of $(Gd_{0.89}La_{0.1})_2Si_2O_7:Ce_{0.02}$ under severe temperature conditions (for example, well logging, nuclear stations, etc.).

■ CONCLUSION

In summary, the combinatorial libraries of blue phosphors $(Gd_{1-x-y}La_x)_2Si_2O_7:Ce_{2y}$ were designed, synthesized, and screened for fast discovery of new type of scintillator material candidates for single crystals, ceramics, glass, and also phosphors. Scaled-up powder synthesis and characterization showed strong evidence that the optimum composition was $(Gd_{0.89}La_{0.1})_2Si_2O_7:Ce_{0.02}$. XRD results show that the La-co-doping samples have a similar structure to the triclinic phase of $Gd_2Si_2O_7$ indexed in standard XRD pattern, exhibiting a strong blue emission under either X-ray or UV excitation. On the basis of the Gaussian fitting of recorded PL and XEL spectra, the emission peaks located at 367 and 387 nm can be attributed to 5d-4f electrons transitions of Ce^{3+} ions. It has been also discovered that the $(Gd_{0.89}La_{0.1})_2Si_2O_7:Ce_{0.02}$ powders possess a very intensive X-ray luminescence, fast decay time of 26.7 ns, and good thermal stability of luminescence at an elevated temperatures up to 200 °C. These characteristics indicate that the optimal $(Gd_{0.89}La_{0.1})_2Si_2O_7:Ce_{0.02}$ composition may have a high potential as varied scintillator materials (in the form of bulk or powder) and the combinatorial screening is a useful tool to discover and develop new compositions or materials of different types.

■ AUTHOR INFORMATION

Corresponding Author
*Phone: +86 021 52412413. Fax: +86 021 52412404. E-mail: qianliu@sunm.shcnc.ac.cn.

Notes
The authors declare no competing financial interest.

■ ACKNOWLEDGMENTS

■ REFERENCES

(1) Inadama, N.; Murayama, H.; Omura, T.; Yamashita, T.; Yamamoto, S.; Ishibashi, H.; Kawai, H.; Omi, K.; Umehara, T.; Kasahara, T. A depth of interaction detector for PET with GSO crystals doped with different amounts of Ce. *IEEE Trans. Nucl. Sci.* **2002**, *49*, 629−633.

(2) Shul'Gin, B.; Melcher, C.; Solomonov, V.; Belykh, T.; Podurovskii, S.; Mikhailov, S.; Kuznetsov, A. Y. Scintillation properties of Lu_2SiO_5:Ce single crystals. *Technol. Phys. Lett.* **1996**, *22*, 197−198.

(3) Cooke, D.; McClellan, K.; Bennett, B.; Roper, J.; Whittaker, M.; Muenchausen, R.; Sze, R. Crystal growth and optical characterization of cerium-doped $Lu_{1.8}Y_{0.2}SiO_5$. *J. Appl. Phys.* **2000**, *88*, 7360−7362.

(4) Tanimori, T.; Kubo, H.; Miuchi, K.; Nagayoshi, T.; Orito, R.; Takada, A.; Takeda, A.; Ueno, M. MeV γ-ray imaging detector with micro-TPC. *New Astron. Rev.* **2004**, *48*, 263−268.

(5) Nishimura, H.; Hattori, K.; Kabuki, S.; Kubo, H.; Miuchi, K.; Nagayoshi, T.; Okada, Y.; Orito, R.; Sekiya, H.; Takada, A. Development of large area gamma-ray camera with GSO (Ce) scintillator arrays and PSPMTs. *Nucl. Instrum. Methods Phys. Res., Sect. A* **2007**, *573*, 115−118.

(6) Kawamura, S.; Kaneko, J.; Higuchi, M.; Yamaguchi, T.; Haruna, J.; Yagi, Y.; Susa, K.; Fujita, F.; Homma, A.; Nishiyama, S. In Floating zone growth and scintillation characteristics of cerium-doped gadolinium pyrosilicate single crystals. *IEEE Nucl. Sci. Symp. Conf. Rec.* **2006**, 1160−1163.

(7) Kawamura, S.; Kaneko, J. H.; Higuchi, M.; Haruna, J.; Saeki, S.; Fujita, F.; Homma, A.; Nishiyama, S.; Ueda, S.; Kurashige, K. Scintillation Characteristics of (Ce 2.5−30 mol%) Single Crystals Prepared by the Floating Zone Method. *IEEE Trans. Nucl. Sci.* **2009**, *56*, 328−330.

(8) Nishiyama, S.; Kawamura, S.; Kaneko, J. H.; Higuchi, M.; Ueda, S.; Kurashige, K.; Ishibashi, H.; Fujita, F.; Homma, A.; Furusaka, M. Improvement of Scintillation Characteristics of FZ Growth Ce:GPS Crystals by Annealing in Air. *Prog.Nucl. Sci. Technol.* **2011**, *1*, 279−281.

(9) Kaneko, J.; Susa, N.; Tsuchida, S.; Watanabe, M.; Miura, S.; Mizuno, T.; Yamauchi, Y.; Hashiba, M.; Oku, T.; Homma, A. Preliminary results on development of a thin GSO scintillator for neutron science. *Nucl. Instrum. Methods Phys. Res., Sect. A* **2004**, *529*, 307−309.

(10) Sidletskiy, O.; Baumer, V.; Gerasymov, I.; Grinyov, B.; Katrunov, K.; Starzhinsky, N.; Tarasenko, O.; Tarasov, V.; Tkachenko, S.; Voloshina, O. Gadolinium pyrosilicate single crystals for gamma ray and thermal neutron monitoring. *Radiat. Meas.* **2010**, *45*, 365−368.

(11) Gerasymov, I.; Sidletskiy, O.; Neicheva, S.; Grinyov, B.; Baumer, V.; Galenin, E.; Katrunov, K.; Tkachenko, S.; Voloshina, O.; Zhukov, A. Growth of bulk gadolinium pyrosilicate single crystals for scintillators. *J. Cryst. Growth* **2011**, *318*, 805−808.

(12) Feng, H.; Xu, W.; Ren, G.; Yang, Q.; Xie, J.; Xu, J.; Xu, J. Optical, scintillation properties and defect study of $Gd_2Si_2O_7$:Ce single crystal grown by floating zone method. *Phys. B: Condens. Matter.* **2013**, *411*, 114−117.

(13) Kawamura, S.; Higuchi, M.; Kaneko, J. H.; Nishiyama, S.; Haruna, J.; Saeki, S.; Ueda, S.; Kurashige, K.; Ishibashi, H.; Furusaka, M. Phase Relations around the Pyrosilicate Phase in the Gd_2O_3−Ce_2O_3−SiO_2System. *Cryst. Growth Des.* **2009**, *9*, 1470−3.

(14) Kawamura, S.; Kaneko, J. H.; Higuchi, M.; Fujita, F.; Homma, A.; Haruna, J.; Saeki, S.; Kurashige, K.; Ishibashi, H.; Furusaka, M. Investigation of Ce-doped $Gd_2Si_2O_7$as a scintillator material. *Nucl. Instrum. Methods Phys. Res., Sect. A* **2007**, *583*, 356−9.

(15) Suzuki, A.; Kurosawa, S.; Shishido, T.; Pejchal, J.; Yokota, Y.; Futami, Y.; Yoshikawa, A. Fast and high-energy-resolution oxide scintillator: Ce-doped $(La,Gd)_2Si_2O_7$. *Appl. Phys. Express* **2012**, *5*, No. 102601.

(16) Youichi, T.; Kaneko, J. H.; Mikio, H.; Moyuru, M.; Hiroyuki, I. Crystal growth and scintillation properties of $La_{0.2}Ce_{0.05}Gd_{1.75}Si_2O_7$(La-GPS) single crystal with triclinic structure. *Opt. Mater.* **2014**, *36*, 665−669.

(17) Gerasymov, Y.; Baumer, V.; Neicheva, S.; Starzhinskiy, N.; Tarasov, V.; Zelenskaya, O.; Sidletskiy, O. Impact of codoping on structure optical and scintillation properties of $Gd_2Si_2O_7$-based crystal. *Funct. Mater.* **2013**, *20*, 15−19.

(18) Executive Office of the President of the United States. Materials Genome Initiative for Global Competitiveness, 2011. http://www.whitehouse.gov/mgi/.

(19) Zhang, K.; Liu, Q.; Shi, Y.; Pan, Y. Combinatorial Optimization of $(Y_xLu_{1−x−y})_3Al_5O_{12}$:Ce$_{3y}$ Green-Yellow Phosphors. *J. Comb. Chem.* **2010**, *12*, 453−457.

(20) Chen, L.; Bao, J.; Gao, C.; Huang, S.; Liu, C.; Liu, W. Combinatorial synthesis of insoluble oxide library from ultrafine/nano particle suspension using a drop-on-demand inkjet delivery system. *J. Comb. Chem.* **2004**, *6*, 699−702.

(21) Wu, Y. T.; RenG, H.; Ding, D. Z.; Yang, F.; Pan, S. Study on the cerium oxidation state in a $Lu_{0.8}Sc_{0.2}BO_3$ host. *J. Mater. Chem.* **2011**, *21*, 17805−17809.

(22) Pidol, L.; Kahn-Harari, A.; Viana, B.; Ferrand, B.; Dorenbos, P.; De Haas, J.; Van Eijk, C.; Virey, E. Scintillation properties of $Lu_2Si_2O_7$:Ce^{3+}, A fast and efficient scintillator crystal. *J. Phys.: Condens. Matter* **2003**, *15*, 2091.

(23) Feng, H.; Ding, D.; Li, H.; Lu, S.; Pan, S.; Chen, X.; Ren, G. Cerium concentration and temperature dependence of the luminescence of $Lu_2Si_2O_7$:Ce scintillator. *J. Alloys. Compd.* **2011**, *509*, 3855−3858.

(24) Xie, R. J.; Hirosaki, N.; Kimura, N.; Sakuma, K.; Mitomo, M. 2-Phosphor-converted white light-emitting diodes using oxynitride/nitride phosphors. *Appl. Phys. Lett.* **2007**, *90*, No. 191101.